NANO CHARACTERIZATION OF MATERIALS

DIETER K. SCHRODER

Department of Electrical Engineering, Arizona State University
Tempe, AZ 85287-5706, USA
schroder@asu.edu

Material characterization is challenged by continuously decreasing device dimensions placing significant demands on characterization instruments and measurement interpretation. Numerous techniques exist and a few are highlighted here. Some of these have existed for a long time, while others have only emerged from the laboratory recently. Generally they are more user-friendly and have reasonable turn-around times. The trend in many techniques is clearly toward characterization of smaller dimensions. Among the myriad of characterization techniques in use today, I will discuss recent advances in transmission electron microscopy (TEM), electron holography, magnetic exchange force microscopy (MExFM), atom probe ion field ion microscopy, and X-ray tomography. They have made significant advances in the last few years and in some cases have produced very impressive results. For example, TEM is now able to generate images with 0.05 nm resolution, allowing display of individual atoms. MExFM in conjunction with magnetic fields has demonstrated vertical resolution of 0.0015 nm. Helium ion microscopy is also highlighted because it contributes a new application of ion beams, which had been largely the domain of Rutherford backscattering. Progress in developing further advances in nm dimensional characterization will, no doubt, continue to satisfy the demand for such measurements in the future.

Keywords: Semiconductor, Characterization, Transmission electron microscopy, Electron holography, Probes, Magnetic exchange force microscopy, Atom probe ion field ion microscopy, X-ray tomography, Helium ion microscopy.

1. Introduction

Many semiconductor characterization techniques developed over the years have been adapted to the small dimensions of shrinking devices. Some of these techniques, e.g., transmission electron microscopy, that were highly specialized have become fairly routinely used. For example TEM specimen sample preparation was very time consuming before the advent of focused ion beam sample cutting. After a brief discussion of resolution limits of the major characterization techniques, I give some examples of methods suitable for the small geometries of nano devices. Aberration correction in *transmission electron microscopy* have progressed to the point where today 0.05 nm resolution is possible. In fact, individual atoms can be observed. In *off-axis electron holography*, highly coherent electron beams from a field emission gun with a positively-biased biprism, generate a hologram between reference and electron waves modulated by the specimen potential in the image plane. In the reconstruction process from the phase information, the sample potential is extracted, *e.g*., the potential distribution in a MOSFET. For force microscopy measurements, magnetic force microscopy is well suited to explore ferromagnetic domains. However, atomic resolution cannot be achieved because data acquisition involves the sensing of long-range magnetostatic forces between tip and sample. *Magnetic exchange force microscopy* overcomes this limitation by using an atomic force microscope with a magnetic tip, allowing the detection of short-range magnetic exchange force between tip and sample spins and the observation of direct magnetic exchange coupling between the spins of the tip atom and sample atom, giving atomic resolution capability combined with spin sensitivity.

In *X-ray tomography* a series of projection images are used to form a 3-dimensional reconstruction of an object. A recent implementation, with X-rays operating in the 8-11 keV energy range with a zone plate with a 50 nm outermost zone width, achieves 60 nm diffraction-limited spatial resolution. By acquiring a series of 2-dimensional images with the sample rotated stepwise, 3D tomographic data can be reconstructed to provide the ability to "see" inside samples. The *atom probe field ion microscope*, a combination of a field ion microscope and a time-of-flight mass spectrometer of single ion sensitivity, is a projection type microscope with *atomic resolution* with a magnification of a few million times. A high electric field "evaporates"

surface atoms of the specimen. The electric field is carefully controlled so that only one atom at a time leaves the specimen. As the analysis progresses, the entire surface layer of atoms on the specimen is removed, exposing the underlying layers and generating a picture of atomic distributions. In the *Helium ion microscope*, with an ion beam energy spread of less than 1 eV, the diffraction effects of the helium ion beam are more favorable than those of an electron beam. Also, the helium ions produce no appreciable sputtering nor sample damage. The helium beam produces secondary electrons and scattered ions, providing material type/density information, allowing the surface composition to be analyzed with very small lateral resolution.

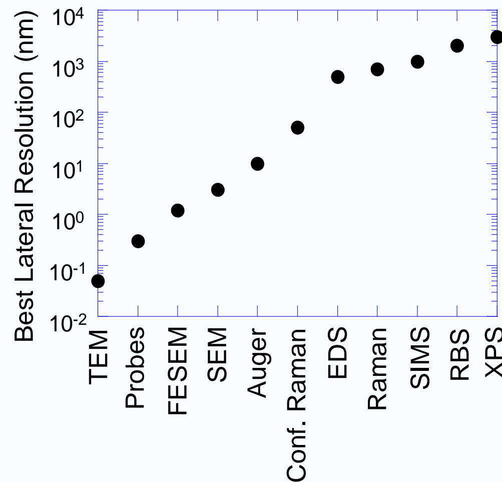

Fig. 1. Best lateral resolution for a variety of characterization techniques. TEM: transmission electron microscope, FESEM: field emission scanning electron microscopy, Conf.: confocal, EDS: energy-dispersive spectroscopy, SIMS: secondary ion mass spectrometry, RBS: Rutherford backscattering spectroscopy, XPS: X-ray photoelectron spectroscopy.

Various measurement techniques show a wide range of lateral resolution as illustrated in Fig. 1. The leading edge technique, as far as resolution is concerned, has been transmission electron microscopy for some time. Recent improvements have pushed its lower limit to about 0.05 nm. As shown in Fig. 1, for resolutions to about 10 nm, electron beam techniques dominate. The only other method allowing atomic resolution is scanning tunneling and atomic force microscopy. Many techniques are used and I will merely describe a few of these: transmission electron microscopy, electron beam holography, magnetic exchange force microscopy, atom probe field ion microscopy, X-ray tomography, and the helium ion microscope.

2. Transmission Electron Microscopy

Feynman, in his 1960 talk and paper *There's Plenty of Room at the Bottom*, stated "…. the electron microscope is 100 times too poor….I put this out as a challenge: Is there no way to make the electron microscope more powerful?"[1] Well, the TEM community has, of course, worked on this problem for many years and through constant improvements has now reached the 0.05 nm lateral resolution limit. In a dedicated scanning TEM (STEM) the effective source size of the electron emitter is de-magnified by the condenser lens system and transferred to the objective lens to focus the beam into a small probe in its back focal plane, where the small electron probe is rastered across an electron transparent specimen. The electrons transmitted through the specimen are then recorded by various detectors as a function of probe position on the sample. Detectors commonly used in a STEM are annular dark-field (ADF), on-axis bright field and secondary electron detectors as well as energy-dispersive X-ray spectrometers and energy-loss spectrometers. One of the benefits of a dedicated STEM is that most of the different detector signals can be acquired simultaneously with pixel-to-pixel correlation.

The resolution limiting factor in STEM has historically been the spherical aberration of the probe forming lenses, particularly the objective lens. Third-order aberration correction revolutionized electron microscopy, allowing materials characterization with unprecedented detail, due to the possibility of using electron probe sizes well below 0.1 nm, leading to significantly increased lateral spatial resolution and increased signal to noise ratio, enabling single atom sensitivity, and higher depth sensitivity providing higher resolution in the vertical direction.

Examples of high-resolution TEM images are shown in Fig. 2. Figure 2(a) shows an annular dark field image of silicon in the <112> zone-axis orientation allowing the 0.078 nm spacing between two adjacent Si columns to be resolved at an electron beam energy of 300 keV.[2] A 0.05 nm resolution image of the 0.14 nm Ge dumbbell structure is shown in Fig. 2(b).[3]

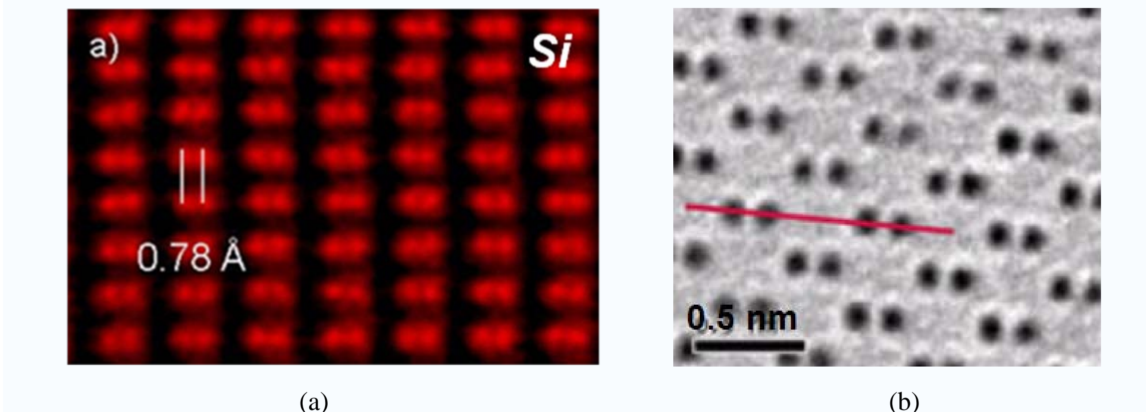

Fig. 2. High-resolution images of (a) silicon in <112> zone-axis orientation[2] and (b) germanium[3].

A bright field STEM image is identical with images recorded by high-resolution TEM (HRTEM), which are based on diffraction interference or phase contrast. Through the use of ADF detectors, Rutherford scattering by the atomic nuclei is the predominant contrast mechanism. This is an incoherent signal because large detector sizes cause an integration of phase contrast effects, *i.e*., different Bragg reflections are integrated to form an image based on total scattered intensity. The cross section is roughly proportional to the square of the atomic number of the scattering element. Hence, this imaging technique is often referred to as *Z*-contrast imaging or high angle ADF (HAADF) imaging. The image formation is incoherent, making images directly interpretable without the need of extensive image simulations.

In STEM *Z*-contrast imaging a small electron probe is scanned across a thin specimen, and the *Z*-contrast image results from mapping the intensity of electrons scattered at high angles reaching the annular detector.[4] The scattering is predominately incoherent and roughly proportional to the square of the atomic number, Z, of the scattering atom. This contrast mechanism can yield images where even small changes in average number are easily discriminated. For a sufficiently small electron beam probe, individual atomic columns are imaged. The high scattering angles break the coherence in the transverse plane, giving a monotonically increasing image intensity with thickness with a brightness determined primarily by their mean square atomic number *Z*. This chemical sensitivity enables different elements to be distinguished at the atomic scale.

An example of this is the interface between a thin HfO_2 layer and a silicon substrate grown by atomic-layer deposition in Figure 3. Electron energy-loss spectroscopy reveals a very thin silicon oxide layer between the HfO_2 and the Si substrate. Small spots of bright contrast, identified as single Hf atoms embedded in the SiO_x structure, can be observed throughout this interlayer in multiple different positions.[5] Using aberration correction, smaller electron probe sizes become available through increase of the illumination angle, allowing thinner sample sections to be in focus leading to higher depth sensitivity. Hence, the acquisition of through focal series effectively becomes equivalent to an optical slicing of the TEM sample and such im-

ages can then be used for three dimensional reconstructions of the structure. Single Hf atoms are in focus at different depths in the recorded image stack. A final reconstruction of the three dimensional interface structure is shown in Figure 3 showing the location of individual HF atoms.[6] Although the lateral spatial resolution is on the order of 0.078 nm, the vertical resolution is on the order of 7-8 nm leading to the cigar-shaped structure of the single Hf atoms.

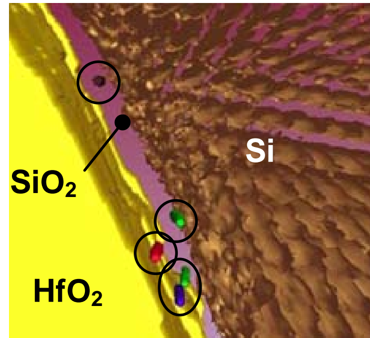

Fig. 3. High-resolution, three-dimensional reconstruction TEM image of the p-Si/HfO_2/SiO_x/Si interface structure. Single Hf atoms are clearly visible inside the SiOx interlayer. The Si atom columns are on the right and the HfO_2 film is on the left. Single Hf atoms are encircled. From K. van Benthem et al.[7]

3. Electron Holography

Electron holography, conceived by Gabor in 1947 to sharpen transmission electron microscopes images, is being applied to map potential distributions in semiconductor devices.[8] The basis for electron holography is that the relative phase of the electron beam after passing through the specimen is determined by comparison with a coherent reference wave. Unlike conventional electron microscope images, represented by the electron wave intensity with no phase information, electron holography allows both phase and amplitude of the coherent wavefront to be determined. The reconstructed phase image provides direct imaging on the nm scale of the electric and magnetic potentials within the sample. Several electron optical geometries have been developed for making electron holograms, but the most popular, the *off-axis, image plane* geometry, is illustrated in Fig. 4(a). It employs an ultrafine ~0.3-0.5 µm diameter conductive fiber, e.g., a gold-coated quartz fiber, the electron biprism,[9] positioned in the imaging lens perpendicular to the electron beam that splits the field of view. A thin TEM specimen is placed over one side of the image field. A positive voltage applied to the fiber bends the electron waves on either side of the fiber toward the center, causing them to overlap and produce interference fringes. The overlapping waves create an interference pattern of parallel fringes. These fringes are changed in position and contrast, depending upon how the specimen affects the electron beam. The pattern is recorded on film or a CCD camera system. A TEM essentially records the amplitude of the electron wave while electron holography allows the extraction of amplitude *and* phase.

In the absence of strong dynamical electron diffraction effects, the phase component is directly related to electrostatic potential, making electron holography useful for 2-dimensional profiling of electrostatic potentials in semiconductor structures. Reconstruction of the phase of the electron wave from the hologram involves Fourier transformation, selection of the sideband in diffraction space and inverse Fourier transformation to produce amplitude and phase maps. The phase yields the potential provided the sample thickness is known. For example, it is possible to display potential contour maps of semiconductor devices without and even with bias by carefully attaching contacts to the TEM specimen. Figure 4(b) shows the cross section and the potential contours within a MOSFET. This figure clearly shows the source/drain, gate, and gate spacer regions.

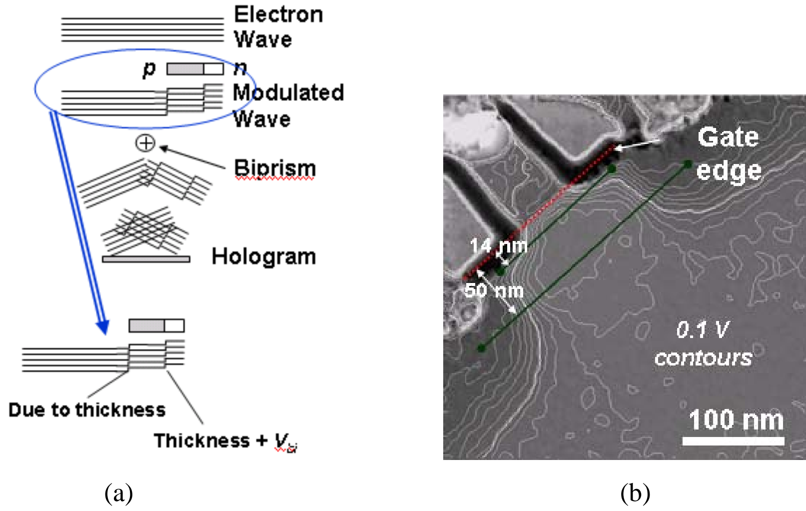

(a) (b)

Fig. 4. (a) Schematic of electron holography, (b) electrostatic potential contour maps of a MOSFET. The separation between adjacent contour lines is 0.1 V. After Han.[10]

Proper sample preparation is very important for minimal sample damage. The sample must be thinned to be electron transparent. Focused ion beam (FIB), commonly used for TEM sample preparation, produces sample damage making quantitative holographic analysis unreliable. The preferred method is wedge polishing, followed by FIB *in-situ* sample lift-out, and back surface low-energy Ar ion milling.[10] One can also determine the two-dimensional carrier concentration profiles by coupling electron holography potential measurements with Poisson's equation. This has led to studies of dopant atom movement during annealing including laser annealing. In one study, it is shown that a short-time laser anneal does not change the doping profile.[11] In the same study electron holography during failure analysis was used to show drain boron dopant depletion near a shallow trench isolation oxide and missed implanted regions.

4. Magnetic Exchange Force Microscopy

In scanning probe microscopy (SPM) a sharp tip is scanned across a sample surface at very small distances to obtain two- or three-dimensional images of the surface at nanometer or better lateral and/or vertical resolution.[12] In the extreme, one can obtain lateral resolution on the order of 0.1 nm and vertical resolution of 0.01 nm or better in some cases. The original application of SPM was the scanning tunneling microscope, invented in 1982.[13] A myriad of SPM instruments has been developed over the past decade or so, and one can sense current, voltage, resistance, force, temperature, magnetic field, work function, light, and so on with these instruments at high resolution. The operation of the instruments is generally based on detecting the near-field image. SPM has been described in many publications[14] and here I only discuss magnetic exchange force microscopy as an example of the power of this technique.

The concept of magnetic exchange force microscopy is shown in Fig. 5 using the example of antiferromagnet nickel oxide, where neighboring {111} planes are aligned antiferromagnetically with nickel spins of opposite orientations (red and green) alternating along <110> directions on the (001) surface. I mention this technique because it illustrates the capability of probe measurements. For MExFM measurements, a cantilever with an iron-coated tip is scanned above the (001) surface. An external magnetic field maximizes the sensitivity of the tip apex to the out-of-plane component of the canted spins of the nickel atoms. Purely chemical and structural contrasts reflect only the arrangement of nickel and oxygen atoms. If the magnetic exchange interaction between the spins of the foremost iron atom at the tip apex and the nickel atom directly below is detected, an additional contrast modulation between neighboring rows of nickel atoms appears.[15]

Force is detected by the frequency-modulation or tapping-mode technique with the cantilever self-oscillating with constant amplitude and tip–sample interactions shifting the cantilever frequency from the resonance frequency of the free cantilever. During x-y plane scans, the frequency change remains constant by adjusting the z position of the tip relative to the surface, permitting atomic resolution on conducting and non-conducting surfaces in the non-contact regime, with height differences in the topographic image reflecting variations of the short-range forces between the tip atom and the atomic species at the surface.

An example of high-resolution probe measurements is shown in Fig. 6, where the AFM images of the antiferromagnetic insulator nickel oxide combine the atomic resolution capabilities of atomic force microscopy with spin sensitivity.[15] This magnetic exchange force microscopy reveals the arrangement of both surface atoms and their spins simultaneously. An external magnetic field aligns the magnetic polarization at the tip apex, allowing the direct magnetic exchange coupling between the spins of the tip atom and sample atom that are closest to each other to be observed. From the line section along the [001] direction the chemical apparent height difference between nickel and oxygen in 6(a) obtained at a relatively large tip–sample distance is about 0.0045 nm. For smaller separation the additional apparent height difference between nickel atoms of opposite spin orientations due to the magnetic exchange interaction with the spin of the iron tip in Fig. 6(b) is 0.0015 nm and gives additional Ni/Ni contrast. The error bars represent the root-mean-square noise after unit cell averaging. These images illustrate the remarkable lateral and even more the vertical spatial resolution of probe measurements.

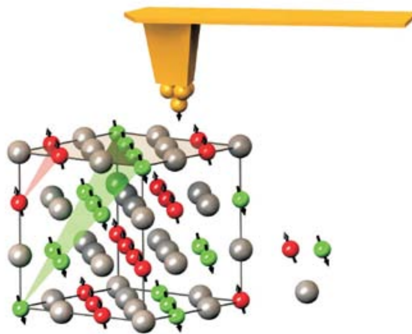

Fig. 5. Concept of magnetic exchange force microscopy of the antiferromagnet nickel oxide. Ni spins of opposite orientations (red and green) alternate along <110> directions on the (001) surface. After Kaiser et al.[15]

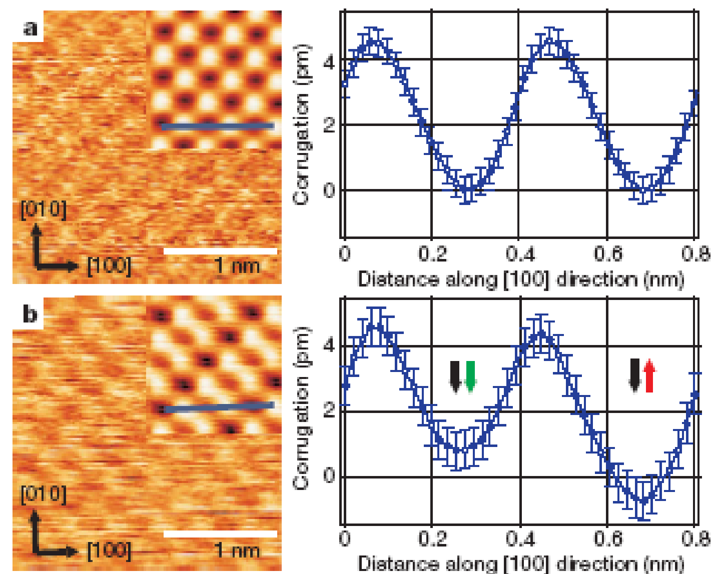

Fig. 6. Raw data are displayed together with an inset tiled from the single chemical (a) and magnetic (b) unit cell. After Kaiser et al.[15]

5. Atom Probe Field Ion Microscopy

The atom probe traces its origins to the field ion microscope (FIM) invented in 1951 by Müller.[16] The basic configuration of a field ion microscope is a needle-shaped specimen positioned approximately 5 cm from a phosphor screen in an ultrahigh vacuum system.[17] Microchannel plate image intensifiers serve as detectors, and are placed immediately in front of the phosphor screen to increase the gain of the image by a factor of ~1000. The specimen is connected to a cryostat and a high voltage supply. After evacuating the vacuum system a trace of image gas is admitted into the system. Both the temperature and base pressure are important parameters in obtaining reliable information from this technique. The choice of the image gas depends on the material being analyzed, and is usually helium for the refractory metals and neon for most other systems.

The principle of the technique is illustrated in Fig. 7. The voltage applied to the specimen is increased until an image appears on the phosphor screen. Due to the enhancement of the field in the vicinity of the apex of the needle-shaped specimen, the image gas atoms are polarized and attracted to the specimen where they become thermally accommodated to the cryogenic temperature. For a sufficiently high electric field, on the order of 37 V/nm for neon, the image gas atoms on the surface of the specimen can be field ionized by an electron tunneling process. As soon as the atoms at the tip become positively charged ions, they are repelled from the positively charged specimen towards the phosphor screen. Upon impacting the phosphor screen they produce a spot of light. This process occurs across the entire surface of the needle, and the resulting pattern on the phosphor screen is the field ion image. The voltage is very carefully controlled so that only one atom at a time leaves the specimen. The ion charge/mass, analyzed by a time-of-flight mass spectrometer, and the spatial location of each ion gives the chemical identity of each atom. One can resolve the chemical identity and position of individual atoms in 3D with atomic resolution in the z direction and sub-nm lateral resolution. Under an identical voltage differential, lighter ions reach the detector faster than heavy ions. To accurately measure the time of departure of the ion, the positive voltage is pulsed. The arrival time of the ion is recorded by a set of timing devices on the single particle detector. This detector operates under the principle of a delay line detector. The time-of-flight of the ion identifies the mass-to-charge of the ion, which provides the elemental identity, so the atomic species is obtained. The numbers of atoms of various elements that hit the detector are recorded and a mass spectrum is determined.

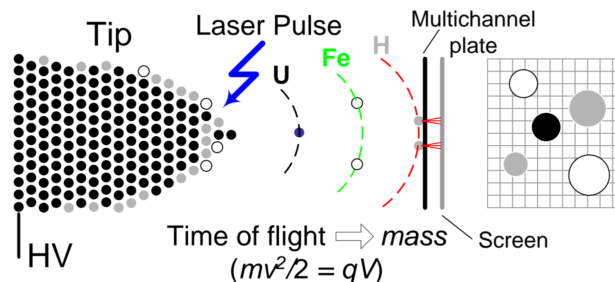

Fig. 7. Schematic of the atom probe.

The location of the atom in the specimen is determined from the ion's hit position on the delay line detector. The x and y coordinates of the hit relate to the ion's original position on the specimen. Since neither potential lines nor atomic flight paths can intersect or cross each other, an ion that hits the detector to the right of another ion must have been located to its right on the specimen. The depth, or z dimension, is provided by the sequence (time) of the ion hits on the detector. Placing the detector at a distance away from the specimen magnifies the tip of the specimen. In due course, atoms from the surface ionize, exposing another layer of atoms under them. This process of field ionization provides a 3D image of the entire specimen. The ions' position in the plane parallel to the specimen surface can be calculated from the two-dimensional hit position of the ion on the detector with a lateral precision approaching 0.5 nm. Since atomic layers erode

predictably from the specimen surface, sequence number can be used to calculate an ion's position in the direction normal to the specimen surface in the original specimen with 0.2 nm resolution.

Various drawbacks plagued the first tools, such as slow collection rates, an extremely small field of view and the need for conducting samples. However, in recent years significant instrumentation advances have been made. Fields of view of more than 100×100 nm are now possible, alongside detection rates exceeding a million atoms per minute. 100 nm sample size and 100 mm viewing screen leads to a 10^7 magnification. Femtosecond pulsed lasers can be used instead of nanosecond pulsed voltages, enabling the atom probe to examine semiconducting and even insulating specimens. Sample preparation is the greatest challenge. Samples must have a tip radius of about 50 nm, and a region of interest located within a few hundred nanometers of the tip. For metallic samples, this is usually possible with electropolishing, but for many semiconductor samples a focused ion beam instrument is the best tool. With this technique, gallium ion beams can mill the sample to the correct shape, with platinum or tungsten protective layers being deposited to protect the sample from ion beam damage. Some instruments also combine a scanning electron microscope with the FIB column, enabling imaging of the sample, to ensure a good tip shape, and accurate positioning of the region of interest near the tip.

Two example images are shown in Fig. 8. Figure 8(a) shows InGaN/GaN quantum wells with the blue (dark) dots representing gallium and the orange (light) dots indium atoms.[18] The analyzed volume is 20x20x100 nm^3 corresponding to a volume of $4x10^{-17}$ cm^3. Figure 8(b) is the image from a boron-doped Si ($N_B=10^{19}$ cm^{-3}) sample with B represented by the green (light) dots and Si by the blue (dark) background.[19] Based on the sampled size of 20x20x5 nm^3 corresponding to a $2x10^{-18}$ cm^3 volume, one would expect to find 20 boron atoms. However, only 11 atoms are evident, illustrating the statistical nature of the dopant atoms.

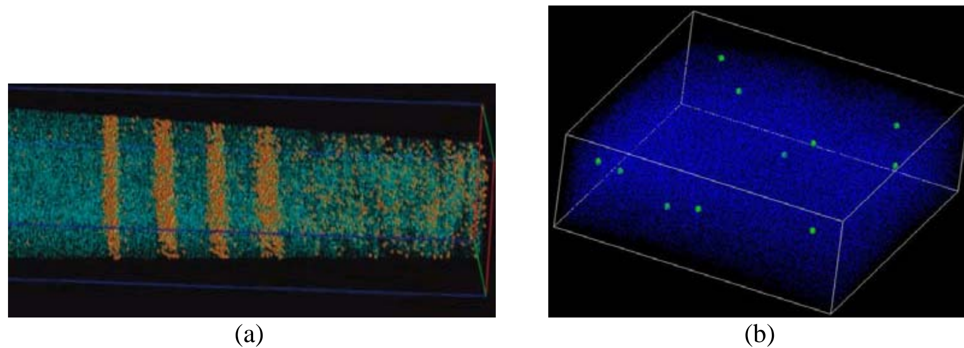

(a) (b)

Fig. 8. (a) InGaN/GaN quantum wells (about 4 nm thick)[18]; (b) 10^{19} cm^{-3} boron in silicon; volume: $2x10^{-18}$ cm^3.
Courtesy of A. Cerezo, Oxford University.[19]

6. X-Ray Tomography

Tomography is the cross-sectional imaging of an object from either transmission or reflection data collected by illuminating the object from many different directions. In X-ray tomography, a branch of X-ray microscopy, a series of projection images are used to calculate a three-dimensional reconstruction of an object. Contrast in transmission X-ray imaging is mainly based on absorption differences between different materials within the sample. It is used in the medical community for non invasive X-ray imaging of the human anatomy. The impact of this technique in diagnostic medicine has been revolutionary, since it has enabled doctors to view internal organs with unprecedented precision. The same technique is used for non-destructive inspections of parts and components with the object viewed in three dimensions using virtual cross sections of internal structures instead of destructive physical cross sectioning. Conventional micro tomography has spatial resolution from a few microns to tens of microns, which is insufficient to observe die level defects in semiconductor devices. High-resolution X-ray microscopy or nanotomography is increasingly used in synchrotron radiation research to characterize biological, composites and nanomaterials.

More recently, the development of the hard X-ray tomographic microscope has been introduced using the Cr-Kα emission line with spatial resolution of 60 nm, and more recently 8 keV Cu-Kα X-rays, enabling 3D tomographic imaging of Cu interconnects through up to 30 µm thick IC silicon die.[20] While suitable preparation techniques for thinning the silicon substrate such as dimpling are well established and widely used, it is highly desirable to use higher X-ray energies to simplify sample preparation and increase penetration for higher angle projections in X-ray tomography.

Its application to high-resolution materials characterization had to await the implementation of X-ray focusing. X-rays are focused with zone plates, which are circular transmission gratings with radially increasing line density and use constructive interference of X rays from adjacent zones to form a focus. The focal length of a zone plate is a function of its diameter, its outermost zone width and the X-ray wavelength. The numerical aperture, given by the maximum diffraction angle, is determined by the outermost zone. X-rays of 2.4 nm wavelength can resolve 25 nm feature size, approximately 10 times better than visible light microscopy.[21] X-ray microscopy is highly sensitive to elements and bonds between atoms, because X-rays interact mainly with inner-shell electrons of atoms.

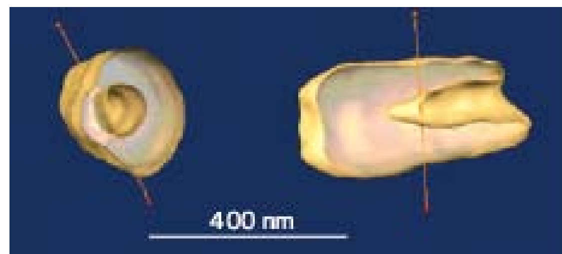

Fig. 9. X-ray tomograph of a tungsten plug obtained from 141 two-dimensional images taken at 1° intervals. A void of 50-80 nm diameter is seen in the approximately 250x500 nm^2 plug. After Yin et al.[26]

High-resolution X-ray tomography is used for biological and materials imaging.[22] Detailed three-dimensional maps, at about 60 nm spatial resolution, of several cryogenically fixed, whole, fully hydrated and unstained biological samples, including individual yeast[23] and bacterium[24] cells, have been produced. Since higher radiation doses are required for nanoscale imaging, radiation sensitive samples such as biological tissue can require cryogenic or other 'fixation' techniques that limit structural damage.[25] X-ray micro and nanotomography offers a powerful technique in non destructive characterization of package and die level defects respectively. Virtual delayering of reconstructed data offers a novel approach towards localization of failures in IC or packages without physical deprocessing. Figure 9 shows a tomographic image of a tungsten plug of an IC interconnect, obtained with X-rays of 0.118 nm wavelength which is just above one of the tungsten absorption edges. Such plugs are prone to failure through the formation of central voids during the deposition process. These X-rays are sufficiently energetic to pass through a silicon layer up to about 50 µm thick, ensuring an appropriately contrasted image. Two-dimensional images with incident X-ray angles from -70° to 70° in 1° increments were taken, with an exposure time of about a minute each.[26]

The current 60-nm limit on spatial resolution is largely a result of the outer-zone width and thickness of the available zone plates, together with restrictions in the depth of field and the limited angular range in the data sets. Two-dimensional images resolved to 15 nm have been achieved in the soft X-ray region[27], albeit with a reduced depth of field. With hard X-rays, 30 nm spatial resolution in two dimensions has been achieved.[28] Higher energy X-rays generally have the advantage of longer focal lengths, allowing a greater working distance. The disadvantage of hard X-rays is the need for thicker zone plates, which are more difficult to fabricate with the requisite narrow outer zones. Nonetheless, there has been steady progress on better zone plates for nanoscale imaging throughout the X-ray region, as well as more sophisticated optics and nano-fabrication techniques.[29]

7. Helium Ion Microscopy

Helium ion microscopy is a relatively recent addition to the family of beam microscopies. It is melding of scanning electron microscopy and Rutherford backscattering. The principle of the technique is illustrated in Fig. 10. A He ion beam is rastered across the sample generating secondary electrons, and backscattered He ions, and transmitted electrons. These are detected and their signals are shown on a 2-dimensional display. An important component of the He ion microscope is the ion source. Helium ion microscopy is related to field ion microscopy in which a positively-biased sharp tip at cryogenic temperature established a very high electric field at its tip.[30] At high tip electric fields, atoms are field evaporated, but at lower fields neutral atoms near the tip are ionized through electron tunneling and the resulting positive ions are immediately accelerated away from the tip. The emission from a single atom at the source tip is selected with an aperture and the beam current can be modulated by changing the gas pressure, which can be controlled over several orders of magnitude without any need to change the beam energy, aperture, focus, extraction field, or beam steering. Under typical conditions, the beam current from a single atom is 10 pA, but operation from 1 fA to 100 pA is practical.

The ion beam energy spread is around 1 eV and the ion beam probe size is on the order of 0.75 nm. Ion beams have less diffraction effects than electron beams due to the higher ion momentum allowing focusing of ion beams to sub micron dimensions. The higher momentum causes the He ions to penetrate deeper into the sample than electrons before dispersing. Although secondary electrons are produced throughout the volume, only the ones near the surface can escape and be detected with small surface area yielding high-resolution images.

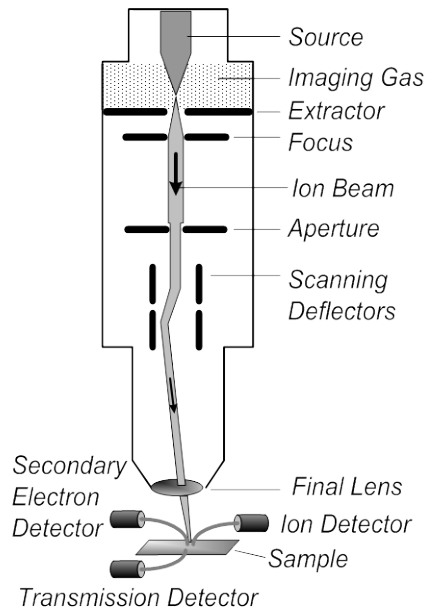

Fig. 10. The Helium ion microscope.[31]

The scanning electron microscope probe size is limited by diffraction and chromatic aberration. The high source brightness and the shorter wavelength of the helium ions allow ion beams to be focused to smaller probe size than in the secondary electron microscope (SEM). The relatively large excitation volume of the electron beam in the substrate limits the resolution of an SEM regardless of the probe size. The excitation volume of the He ion beam is much smaller, especially at and near the surface where secondary electrons originate. SEMs are typically operated at or near their secondary electron unity crossover point to minimize sample charging, yielding one secondary electron per incident electron. Typically for each incoming He ion from 2 to 8 secondary electrons are generated, allowing for high contrast imaging.

The He ion microscope detects secondary electrons and Rutherford backscattered He ions (RBI). The secondary electron yield varies considerably from one material to another and is higher for He ions than for incident electrons leading to higher signal-to-noise ratio. The backscattered ion energy is related to the mass of the target atoms (heavier target nuclei lead to more energetic backscattered helium ions) and the backscattering angle making the He ion microscope capable of mapping sample atomic number, similar to Rutherford backscattering but with nanometer lateral resolution. Figure 11 shows secondary electron and RBI images of a solder bump with the RBI image providing more atomic mass detail.[32] Helium ions also provide crystallographic information as the generated electrons or scattered ions depend on the angle between the incident He ion beam and the sample crystalline orientation. The low-energy He ions, typically in the 30-50 keV range, do not generate X-rays, however, and hence do not provide X-ray images, the way secondary electron microscopes do.

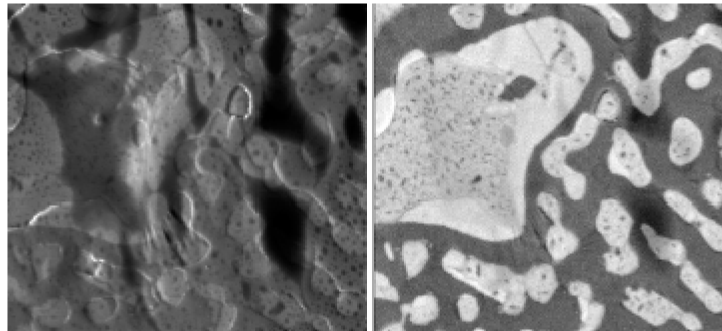

Fig. 11. (a) Secondary electron image of a solder bump showing topography, but little material difference, (b) RBI image clearly showing the difference between areas of tin (dark) and lead (light). After Morgan et al.[32]

8. Conclusion

I have discussed several characterization techniques that have recently been developed for either lateral and/or vertical high-resolution measurements. High resolution is usually, but not always, in the nm or sub nm range. These techniques are transmission electron microscopy, electron beam holography, magnetic exchange force microscopy, atom probe field ion microscopy, and X-ray tomography. TEM, with third-order aberration correction, allows individual atoms to be displayed with an example of Hf atoms in a silicon-oxide oxide matrix. Electron holography allows the potentials within semiconductor devices to be displayed even with applied external bias. It is further used to determine lateral doping profiles and has been used in that mode during failure analysis. Magnetic exchange force microscopy is included as an example of extending the range of atomic force microscopy, when coupled with a magnetic field, into the range of 0.0015 nm vertical resolution. Atom probe field ion microscopy, through appropriate sample preparation of sharply-pointed needles, is used to show the distribution of individual atoms within a matrix of other atoms. It has very high lateral and vertical resolution. X-ray tomography, routinely used for medical imaging to “look into” the body or head, has also been adopted by the semiconductor community and can be used to look into regions of a semiconductor device or interconnects. Helium ion microscopy is briefly mentioned as it is a relatively new technique. Its application is typically in those areas where SEM is also used. It has the advantages over SEMs of secondary electron and scattered He ion imaging, smaller probe size, higher secondary electron yield, and higher sensitivity to sample mass.

No doubt we will continue to see further developments in these and other characterization techniques. In electron microscopy there will be enhancements in electron sources, the application of aberration correction technology to lenses, and more selective detector systems. Focused ion beam (FIB) systems have evolved to become a critical tool in sample preparation. Present generation ion optical systems feature 5 nm spot size for imaging and nanomachining, making the FIB system an ideal tool for electron-transparent sample preparation for atomic resolution TEM/scanning TEM imaging,

chemical and electrical analysis. By allowing contacts to be made in the FIB tool to these very small and very thin samples, full STEM based electrical characterization using electron beam induced current, cathodoluminescence, and electron holography of biased devices is possible. Magnetic resonance imaging (MRI), a powerful imaging technique based on the manipulation of nuclear spins with radio-frequency fields and their subsequent detection with induction-based techniques, typically operates on the scale of millimeters to micrometers. Magnetic resonance force microscopy uses force detection to overcome the sensitivity limitations of conventional MRI, with spatial resolution better than 100 nm. Three-dimensional characterization of semiconductor devices at the near atomic level is increasingly important, especially for semiconductor logic and memory devices as well as quantum structured solar cells. Chemical resolution down to the ppm level is needed while maintaining sub-nm spatial resolution. Atom probe tomography is capable of these detection levels and will continue to make advances by utilizing advanced FIB sample preparation. These are merely a few examples of future advances. Many others will emerge as the need arises.

9. Acknowledgments

I thank many people for many characterization discussion over the years. For this paper I thank K. van Benthem (Oak Ridge National Labs.), M.G. Han (Arizona State University), M. Gribelyuk (IBM), S.H. Lau (Xradia Inc.), and J. Morgan (Alis Corp.) for enlightening discussions and several others for permission to use their figures.

10. References

[1] R.P. Feynman, There's plenty of room at the bottom, *Eng. Sci. Mag.* **23**(5), 22-36 (1960).
[2] K. van Benthem, Y. Peng and S. J. Pennycook, Tomographic imaging of nanocrystals by aberration-corrected scanning transmission electron microscopy *Mat. Res. Soc. Symp. Proc.* **839**, 3-7, (2005).
[3] Source: FEI Co.
[4] S.J. Pennycook and D.E. Jesson, High-resolution incoherent imaging of crystals, *Phys. Rev. Lett.* **64**(8), 938-941 (1990).
[5] K. van Benthem, A.R. Lupini, M. Kim, H.S. Baik, S.J. Doh, J.H. Lee, M.P. Oxley, S.D. Findlay, L.J. Allen, J.T. Luck and S.J. Pennycook, Three-dimensional imaging of individual hafnium atoms inside a semiconductor device, *Appl. Phys. Lett.* **87**(3), 034104-1-3 (2005).
[6] K. van Benthem and S. Pennycook, Aberration-corrected scanning transmission electron microscopy for atomic-scale characterization of semiconductor devices in *Analytical and Diagnostic Techniques for Semiconductor Materials Devices, and Processes 7* (D.K. Schroder, L. Fabry, R. Hockett, H. Shimizu and A. Diebold, eds.), *ECS Trans.* **11**, 225-231 (2007).
[7] K. van Benthem, A.R. Lupini, M.P. Oxley, S.D. Findlay, L.J. Allen and S.J. Pennycook, Three-dimensional ADF imaging of individual atoms by through-focal series scanning transmission electron microscopy, *Ultramicroscopy* **106**(11/12), 1062-1068 (2006).
[8] E. Völkl, L.F. Allard and D.C. Joy, *Introduction to Electron Holography* (Kluwer, New York, 1999).
[9] G. Möllenstedt and H. Düker, Observations and measurements on biprism-interferences with electron waves (in German), *Z. Physik* **145**, 377-397 (1956).
[10] M.G. Han, P. Fejes, Q. Xie, S. Bagchi, B. Taylor, J. Conner and M.R. McCartney, Quantitative analysis of 2-D electrostatic potential distributions in 90-nm Si pMOSFETs using off-axis electron holography, *IEEE Trans. Electron Dev.* **54**(12), 3336-3341 (2007).
[11] M. Gribelyuk, A.G. Domenicucci, P.A. Ronsheim, J.S. McMurray and O. Glushenkov, Electron holography as a characterization tool for 2-D analysis of p-n junctions, in *Analytical and Diagnostic Techniques for Semiconductor Materials Devices, and Processes 7* (D.K. Schroder, L. Fabry, R. Hockett, H. Shimizu and A. Diebold, eds.), *ECS Trans.* **11**, 225-231 (2007).
[12] D.A. Bonnell, *Scanning Probe Microscopy and Spectroscopy*, 2nd Ed. (Wiley-VCH, New York, 2001).
[13] G. Binnig, H. Rohrer, C. Gerber, and E. Weibel, "Surface studies by scanning tunneling microscopy," *Phys. Rev. Lett.* **49**, 57-60 (1982); G. Binnig and H. Rohrer, "Scanning tunneling microscopy," *Surf. Sci.* **126**, 236-244, (1983).
[14] For example: E. Meyer, H.J. Hug, and R. Bennewitz, *Scanning Probe Microscopy, the Lab on a Tip* (Springer, Berlin, 2004); A.S. Foster and W.A. Hofer, *Scanning Probe Microscopy, Atomic Scale Engineering by Forces and Currents* (Springer, Berlin, 2006); K.S. Birdi, *Scanning Probe Microscopes, Applications in Science and Engineering* (CRC Press, Boca Raton, 2003).
[15] U. Kaiser, A. Schwarz, and R. Wiesendanger, "Magnetic exchange force microscopy with atomic resolution," *Nature*, **446**(7135), 522-525 (2007).

[16] E. W. Müller, The field ion microscope. *Z. Physik* **131**, 136–142 (1951).
[17] M. K. Miller, The development of atom field-ion microscopy**,** *Mat. Charact.* **44**(1/2), 11–27 (2000); T.F. Kelly and M.K. Miller, Atom probe tomography, *Rev. Sci. Instrum.* **78**, 031101 1-20 (2007).
[18] M. Galtrey, R. Oliver, and C. Humphreys, Atom probe provides evidence to question InGaN cluster theory, *Compound Semicond.* **13**(4), 27-30 (2007).
[19] http://www.materials.ox.ac.uk/fim/whatis3dap.html
[20] S.H. Lau, A. Tkachuk, M. Feser, H. Cui, F. Duewer, W. Yun and D. Vallet, Non destructive failure analysis technique with a laboratory based 3D X-ray nanotomography system, *LSI Testing Symp.* (2006).
[21] G. Schneider, T. Schliebe and H. Aschoff, Cross-linked polymers for nanofabrication of high-resolution zone plates in nickel and germanium, *J. Vac. Sci. Technol*. B 13(6), 2809-2812 (1995).
[22] D. Attwood, Microscopy: Nanotomography comes of age, *Nature* **442**(7103), 642-643 (2006).
[23] C.A. Larabell and M.A. Le Gros, X-ray tomography generates 3-D reconstructions of the yeast, saccharomyces cerevisiae, at 60-nm resolution, *Mol. Biol. Cell* **15**(5), 957–962 (2004).
[24] M.A. Le Gros, G. McDermott and C.A. Larabell, X-ray tomography of whole cells, *Curr. Opin. Struct. Biol.* **15**(5), 593–600, 2005.
[25] G. Schneider, Cryo X-ray microscopy with high spatial resolution in amplitude and phase contrast, *Ultramicroscopy* **75**(2), 85-104 (1998).
[26] G.C. Yin, G.C. Yin, M.T. Tang, Y.F. Song, F.R. Chen, K.S. Liang, F.W. Duewer, W. Yu, C.H. Ko and C.H. Shieh, Energy-tunable transmission x-ray microscope for differential contrast imaging with near 60 nm resolution tomography, *Appl. Phys. Lett.* **88**(24), 241115 1-3 (2006).
[27] W. Chao, B. Harteneck, J. Liddle, E. Anderson and D. Attwood, Soft X-ray microscopy at a spatial resolution better than 15 nm**,** *Nature* 435(7046), 1210–1213 (2005).
[28] Tang, M.-T. *et al.* in *Proc. 8th Int. Conf. X-ray Microscopy* (eds. Aoki, S., Kagoshima, Y. & Suzuki, Y.) 15 (IPAP, Tokyo, 2006).
[29] E.D. Fabrizio, F. Romanato, M. Gentili, S Cabrini, B. Kaulich, J. Susini and R. Barrett, High-efficiency multilevel zone plates for keV X-rays, *Nature* 401(6756), 895–898 (1999); T. Wilhein, B. Kaulich and J. Susini, Two zone plate interference contrast microscopy at 4 keV photon energy, *Optics Commun.* 193(1/6), 19–26 (2001); C. Chang, A. Sakdinawat, P. Fischer, E. Anderson and D. Attwood, Single-element objective lens for soft x-ray differential interference contrast microscopy, *Opt. Lett.* 31(10), 1564–1566 (2006).
[30] V. N. Tondare, Quest for high brightness, monochromatic noble gas ion sources, *J. Vac. Sci. Technol.* **A 23**(6), 1498-1508 (2005).
[31] http://www.aliscorporation.com/technology/tech-demo.asp.
[32] J. Morgan, J. Notte, and B. Ward, An introduction to the He ion microscope, *Microscopy Today*, **14**(4), 24-31 (2006).